Available online at www.sciencedirect.com
SCIENCE DIRECT®
International Journal of Heat and Mass Transfer 48 (2005) 5255–5269
International Journal of HEAT and MASS TRANSFER
www.elsevier.com/locate/ijhmt

Heat transfer and film-cooling for the endwall of a first stage turbine vane

Karen A. Thole *, Daniel G. Knost

Department of Mechanical Engineering, Virginia Polytechnic Institute and State University, Blacksburg, VA 24060, USA

Received 2 March 2005; received in revised form 20 July 2005
Available online 4 October 2005

Abstract

Secondary flows that result in turbomachines from inherent pressure gradients in airfoil passages, are the main contributors to aerodynamic losses and high heat transfer to the airfoil endwalls. The endwalls present a challenge to durability engineers in maintaining the integrity of the airfoils. One means of preventing degradation in the turbine is to film-cool components whereby coolant is extracted from the compressor and injected through small cooling holes in the airfoil surfaces. In addition to film-cooling, leakage flows from component interfaces, such as the combustor and turbine, can provide cooling in localized areas but also provide a change to the inlet boundary condition to the passage. This paper presents measurements relevant to the endwall region of a vane, which indicate the importance of considering the inlet flow condition.

1. Introduction

Gas turbine engines have become an integral part of our daily lives through propelling aircraft, tanks, and large naval ships and providing power to the electrical grid. To continue the growth of this industry through improvements in engine efficiencies and reducing pollutants, knowledge is needed on how to further designs of the cooling schemes for the hot turbine section. The power output and efficiency of a turbine engine are a direct function of the fluid temperature entering the hot turbine section. Having an optimal cooling scheme for the turbine section reduces the need to extract compressed air from flow that could have been used as hot working fluid for the turbine or can allow even hotter temperatures to enter the turbine.

Turbine inlet conditions in a gas turbine engine generally consist of temperature and velocity profiles that vary in the spanwise and pitchwise directions resulting from combustor exit conditions. These non-uniform profiles have a strong influence on the nature of the secondary flows in the endwall region. Secondary flows refer to velocity components not aligned with the inviscid flow through the airfoil passages. Driving the secondary flows are two pressure gradients: the inherent pressure gradient from turning the flow and the pressure gradient resulting from non-uniform inlet conditions along the radial span of the airfoil passage. The primary components of these secondary flow patterns include a leading edge horseshoe vortex and a passage vortex. The leading edge horseshoe vortex is formed as the incoming boundary layer approaches the stagnation region of the vane. This horseshoe vortex separates into pressure-side and

* Corresponding author. Tel.: +1 5402317192; fax: +1 5402319100.
E-mail address: thole@vt.edu (K.A. Thole).

0017-9310/$ - see front matter © 2005 Elsevier Ltd. All rights reserved.
doi:10.1016/j.ijheatmasstransfer.2005.07.036

Nomenclature

C	true chord of stator vane
C_a	axial chord of stator vane
I	momentum flux ratio
$\dot{m}$	mass flowrate
M	mass flux ratio
P	vane pitch; hole pitch
P_0, p	total and static pressures
Re	Reynolds number
s	surface distance along vane measured from flow stagnation
S	span of stator vane
St	Stanton number
T	temperature
x, y, z	local coordinates
u, v, w	local velocity components
U	velocity magnitude

Greek symbols

η	adiabatic effectiveness, $\eta = (T_\infty - T_{aw})/(T_\infty - T_c)$
ρ	density
ν	kinematic viscosity

Subscripts

aw	adiabatic wall
c	coolant conditions
inlet	inlet conditions
s	streamline distance
∞	freestream conditions

suction-side horseshoe vortex legs. The passage vortex, having the same sense of rotation as the pressure side horseshoe vortex, develops as the flow is turned by the turbine vane or rotor blade. Secondary flows cause aerodynamic losses, high convective heat transfer, and make it difficult to film-cool the endwall.

One method of combating the high convective heat transfer rates for turbine components is through the use of film-cooling holes whereby the air that has been extracted from the compressor, bypasses the combustor, and is injected through discrete holes in the turbine airfoils. One of the more difficult regions to cool is the endwall because of the previously described secondary flow pattern that develops in the airfoil passages. Film-cooling hole placement, particularly in the endwall region, has traditionally been based upon designer experience. Another consideration when designing an effective cooling hole pattern for the endwall of an airfoil is the coolant coverage that can occur from leakage flows at the combustor-turbine interface. These leakage flows are inherent to most turbine systems and do represent a potential cooling source for endwalls, but also represent a change to the inlet boundary condition for the passage and as such these leakage flows need to be assessed in terms of their overall impact to the secondary flows that develop in the turbine endwall region.

The goal of this research was twofold. The first goal was to compare the effects of injecting different coolant flow rates through a two-dimensional slot upstream of an endwall with a turbine vane design. This flow rate represents the leakage flow through a combustor-turbine interface. The second goal was to compare what effect the leakage flow has on the downstream film-cooling injection. This second goal is particularly relevant for those designing film-cooling hole patterns who need to know whether the leakage flow should or should not be considered in their design. This paper contains a summary of relevant past literature, a description of the two different endwall film-cooling hole patterns and experimental set-up used to measure endwall effectiveness levels, and then a summary of the results.

1.1. Relevant factors for endwall flowfield development

An understanding of passage secondary flows has been the subject of research in the gas turbine industry for many years [1]. In an original study, Hawthorne [2] used the vorticity equation, or what is commonly referred to as the Helmholtz equation, to describe how the secondary streamwise vorticity relates to the spanwise (or radial in the case of an annular cascade) total pressure gradient. Flow models that have been proposed from experiments done with uniform temperature profiles and turbulent endwall boundary layers have included the formation of a passage vortex. In the flow model by Langston [3], he depicted a horseshoe vortex that is split into two legs with one on the suction and one on the pressure sides of the airfoils as shown in Fig. 1. Langston indicated a pitchwise pressure gradient in which there is a crossflow from the pressure towards the suction side of the airfoil. In the inviscid limit, this crossflow will occur because of the difference in pressure across the pitch. The spanwise total pressure gradient, resulting from the boundary layer, along with the cross flow promotes the pressure side leg of the horseshoe vortex into forming a passage vortex. The suction side leg exits the blade row as a counter-rotating vortex inside the passage vortex.

Sharma and Butler [4] showed a similar flow model with the primary difference being that the suction side

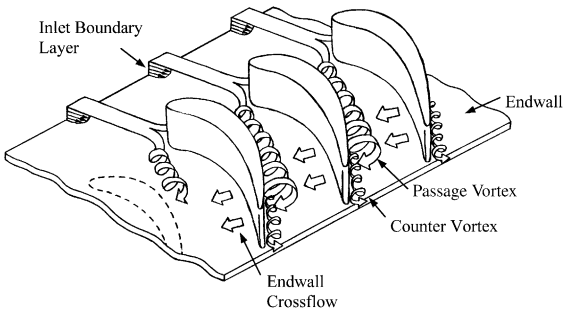

Fig. 1. Secondary flow model presented by Langston [3].

horseshoe vortex begins to lift off the endwall at the minimum pressure along the blade and orbit about the passage vortex. Goldstein and Spores [5] showed that the suction leg remains distinct rising along the span of the turbine blade above the passage vortex. In general, there are some slight disagreements in the different flow models that have been proposed but, for the most part, these flow models, which are primarily based on uniform inlet profiles except for the turbulent endwall boundary layers, agree on the existence of the leading edge and passage vortices.

Experimental flowfield data presented by Bailey [6], Moore et al. [7], Gregory-Smith and Cleak [8], and Kang et al. [9] have all quantified some aspects of the secondary flows. All of these studies, however, have had an inlet boundary condition of a uniform flow except for a turbulent endwall boundary layer such as that shown in Fig. 2. Fig. 3a shows the secondary flowfield vectors, as reported by Kang and Thole [9], for a case with a uniform temperature field and a turbulent boundary layer that had a thickness which was 9% of the span and a momentum Reynolds number of 3340. These measurements, where the location is illustrated on the turbine vane inset, agree with the Langston model. The presence of the passage vortex is quite clear as well as remnants of the leading edge horseshoe vortex on the suction side of the airfoil. The passage vortex also has an effect on the streamwise velocities as shown by the contours.

As previously discussed, combustor exit profiles (first-stage turbine stator vane inlet profiles) are far from uniform in temperature, pressure, and velocity. Some typical profiles are given in the literature by Suo [10], Halls [11], and computed by Crocker et al. [12]. As shown in the literature, downstream of dilution jets, which are typically used to promote mixing in a combustor design, distinct radial and circumferential variations in the velocity field, and total pressure field can be expected. The effect of non-uniform inlet profiles was first considered by Lakshminarayana [13] who gave a generalized expression for secondary vorticity of flows having gradients of temperature, pressure or velocity. Lakshminarayana [13] showed that when considering a uniform temperature profile and a varying velocity profile (such as a turbulent boundary layer), one obtains a passage vortex with a clockwise rotation when looking towards the downstream of the vane passage (similar to the data shown in Fig. 3a). Alternatively, when considering a uniform velocity profile and a varying temperature profile with a maximum temperature at the midspan, Lakshminarayana proposed that one

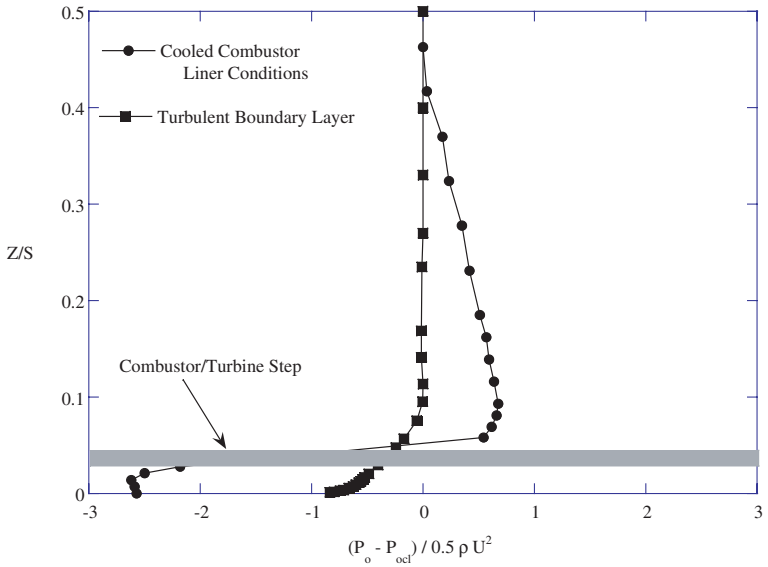

Fig. 2. Comparisons of total pressure profiles of a turbulent boundary layer with that representative of leaving a gas turbine combustor prior to entering the turbine section.

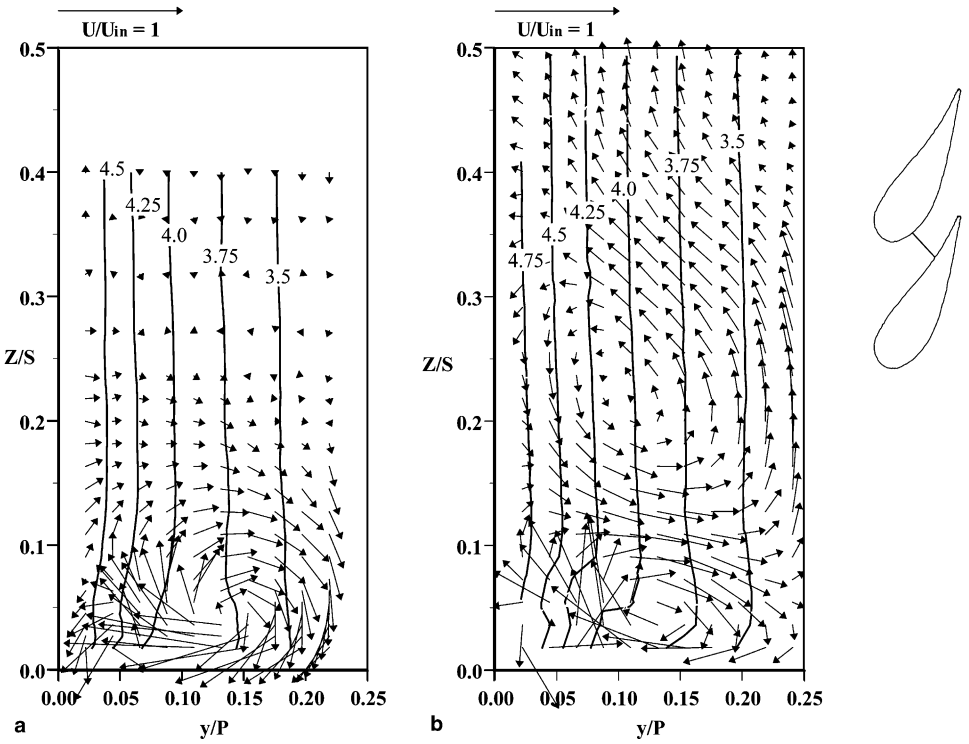

Fig. 3. (a) Measured secondary flows in a turbine vane passage with a two-dimensional turbulent boundary layer [9] and (b) for a case simulating the upstream effects of a combustor liner with combustor-turbine leakage flow [15].

would obtain a passage vortex with a counter-clockwise rotation. This change in rotation results from a change in the sign of the pressure gradient.

While effects of temperature and velocity profiles were shown theoretically by Lashminarayana [13], a change in rotation of the passage vortex was shown computationally by Hermanson and Thole [14]. The computational results for a case with an isothermal flow and turbulent boundary layer were directly comparable to the experimental results given in Fig. 3a with the classic clockwise rotation of the passage vortex. For a varying temperature profile with a maximum temperature at the mid-span location, the lower fluid density results in a lower total pressure at the mid-span when considering a constant static pressure. For this latter case, the rotation of the passage vortex was predicted to be counter-clockwise since the total pressure was lower towards the mid-span. The experimentally measured secondary flows by Colban et al. [15] in Fig. 3b shows what one might expect for an actual turbine where the upstream boundary layer is film-cooled in the combustor section and there is a backward facing slot flow at the combustor-turbine interface. Note that the inlet total pressure profile for a film-cooled combustor is also indicated in Fig. 2 with a total pressure peak (caused by the combustor film-cooling) that is at approximately 10% of the span. The peak in the total pressure causes flow to be directed both downward, towards the endwall, and upward, towards the vane mid-span. As a result a tertiary vortex is formed that convects through the passage.

The above effects are important as one considers the work presented in this paper whereby there is a flush slot present upstream of the turbine endwall with coolant flowing from it. This coolant is referred to as a leakage flow since it represents the leakage that occurs between the combustor-turbine interface.

1.2. Endwall heat transfer resulting from secondary flows

While secondary flows lead to increased aerodynamic losses in the turbine section, surface heat transfer increases resulting from secondary flows is equally as important. Data reported by Kang et al. [16], as well as others, show that the peak heat transfer on the endwall sweeps from the pressure side of the airfoil to the suction side of the adjacent airfoil as the passage vortex moves in that direction. Flow field and heat transfer measurements indicate that the peak in heat transfer coincides with the peak value of the downward velocity vector associated with the vortices that are present. Fig. 4a shows contours of Stanton numbers measured

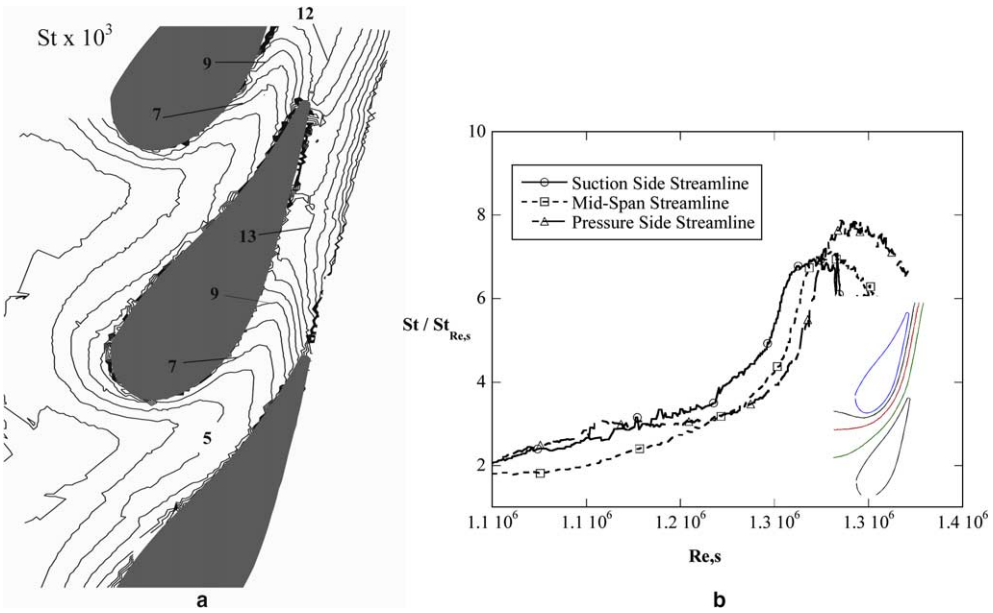

Fig. 4. (a) Measured heat transfer coefficients in terms of Stanton numbers based on the inlet velocities on the endwall [16] and (b) local augmentations of Stanton number for three streamlines along the vane passage.

along the endwall where Stanton number is defined using the incident velocity at the inlet. A region of high heat transfer is observed in front of the vane stagnation location as a result of the formation of the horseshoe vortex. The passage vortex shown in the flowfield measurements in Fig. 3a, causes high heat transfer levels along the vane endwall. Moving into the passage, the heat transfer contours show that the peak Stanton number contours are swept toward the suction surface. Farther into the vane passage, the Stanton number contours become aligned parallel to the direction of flow.

To gain an appreciation for how high the heat transfer coefficients are, Fig. 4b compares the heat transfer augmentation on the endwall induced by the secondary flows. The numerator in the augmentation plot is values taken along streamlines in the mid-passage, near the pressure side, and near the suction side of the vane. These streamline locations were defined through a CFD prediction of an inviscid flow through the vane passage. The denominator, St_{Res}, is the Stanton number predicted from a correlation for a flat plate boundary layer for that given Reynolds number. For this analysis the inlet velocity is used as the scaling velocity. Given the flow acceleration through the passage, one would expect a higher Stanton number to occur as one progresses through the passage. Taking this acceleration into account, the increase in Stanton number would only be a factor of 1.4 given the acceleration through the passage was 5.5 times in the inlet velocity. As noted by Fig. 4b for the three different streamlines (pressure side, midspan, and suction side), the augmentation in heat transfer is on the order of eight times what one would expect from a flat plate correlation. It is also expected that the endwall heat transfer would be severely underpredicted based on this analyses if one were to apply a simple two-dimensional boundary layer code along the streamlines through the passage. As is expected, the pressure and suction side augmentations are similar at the inlet to the vane passage, but as the passage vortex moves toward the suction side, there are higher augmentations near the suction side of the passage.

1.3. Endwall cooling studies

There have been a number of studies documenting endwall cooling from the leakage gap at the turbine-combustor junction and fewer studies that have addressed endwall film-cooling. There have been only two studies presented in the literature that has combined endwall film-cooling with coolant leakage from an upstream slot.

Blair [17] was the first to measure adiabatic surface temperatures and heat transfer coefficients for a range of blowing ratios through a flush slot placed just upstream of the leading edge of his single passage channel. Adiabatic surface temperatures are generally used in gas turbine heat transfer problems where there is a coolant temperature, freestream temperature, and wall temperature. Quantifying the adiabatic surface temperature provides an exact measure of the driving temperature difference present at that surface location. One of the key findings was that the endwall adiabatic effectiveness

distributions showed extreme variations across the vane gap with much of the coolant being swept across the endwall toward the suction side corner. Granser and Schulenberg [18], Colban et al. [15], and Zhang and Moon [19] all reported similar adiabatic effectiveness results in that higher values occurred near the suction side of the vane relative to the pressure side. Based on their measurements, Roy et al. [20], however, indicated that the coolant migrated toward the pressure side of the vane. Their measurements indicated reduced values of local heat transfer coefficients at the leading edge when slot cooling was present relative to no slot cooling.

A series of experiments have been reported for various injection schemes upstream of a nozzle guide vane with a contoured endwall by Burd and Simon [21], Burd et al. [22], and Oke et al. [23]. In the studies presented by Burd and Simon [21], Burd et al. [22] and Oke et al. [23] coolant was injected from an interrupted, flush slot that was inclined at 45° just upstream of their vane. Similar to others, they found that most of the slot coolant was directed toward the suction side at low slot flow conditions. As they increased the percentage of slot flow to 3.2% of the exit flow, their measurements indicated better coverage occurred between the airfoils.

Detailed endwall film cooling results have been conducted by Friedrichs et al. [24–26] and Knost and Thole [27,28]. The results of the studies by Friedrichs et al. indicated a strong influence of the secondary flows on the film cooling and an influence of the film-cooling on the secondary flows. Their data showed that the angle at which the coolant leaves the hole did not dictate the coolant trajectory except near the hole exit. Furthermore the endwall cross-flow was altered so that the cross-flow was turned toward the inviscid streamlines, which was an effect of the film-cooling injection.

The only studies to have combined an upstream slot with film-cooling holes in the passage of the vane were those of Kost and Nicklas [29] and Nicklas [30], a CFD study [27] and an experimental study [28] by the same authors as this paper. One of the most interesting results from the Kost and Nicklas [29] and Nicklas [30] studies was that they found for the slot flow alone, which was 1.3% of the passage mass flow, the horseshoe vortex became more intense. This increase in intensity resulted in the slot coolant being moved off of the endwall surface and heat transfer coefficients that were over three times that measured for no slot flow injection. They attributed the strengthening of the horseshoe vortex to the fact that for the no slot injection the boundary layer was already separated with fluid being turned away from the endwall at the injection location. Given that the slot had a normal component of velocity, injection at this location promoted the separation and enhanced the vortex. Their adiabatic effectiveness measurements indicated higher values near the suction side of the vane due to the slot coolant migration.

Knost and Thole [27,28] reported that the slot coolant flow adequately cooled portions of the endwall and that near the suction side of the vane, the film-cooling holes were redundant in these regions. Measurements also showed two regions were very difficult to cool that included the leading edge region and the pressure side-endwall junction region. As the momentum flux ratios were increased for the film-cooling jets in the stagnation region, the coolant was shown to impact the vane and wash back down onto the endwall surface as a result of the horseshoe vortex. Along the pressure side of the vane in the upstream portion of the passage, the cooling jets were shown to separate from the surface rather than penetrate towards the pressure surface. In the downstream portion of the passage, the jets along the pressure side of the vane penetrated to the vane surface thereby eliminating any uncooled regions at the junction. The measurements were also combined with computations to show the importance of considering the trajectory of the flow in the near-wall region, which was highly influenced by slot leakage flows.

2. Experimental methodology

For the results presented in this paper, adiabatic surface temperatures were spatially-resolved and are presented in non-dimensional adiabatic effectiveness levels. Adiabatic surface temperatures indicate the location of the coolant and are useful in assessing the cooling performance of film-cooling designs. These adiabatic surface temperatures were measured for a range of experimental conditions for a scaled up vane endwall having film-cooling holes and a upstream slot. The advantage of a large scale test rig is that it provides the possibility to achieve highly-resolved spatial data. The experiments for this study were performed in a low speed, closed-loop wind tunnel facility, shown in Fig. 5a that has previously been described by Barringer et al. [31] and Colban et al. [15]. The flow in the wind tunnel is driven by a 50 hp axial vane fan, which is controlled by a variable frequency inverter. Downstream of the fan, the flow is turned by a 90° elbow and passes through a primary flow, finned-tube heat exchanger used to cool the bulk flow. After being turned by another 90° elbow, the flow encounters a three-way flow split. This flow split is controlled by a perforated plate that was designed to obtain the proper pressure drop in the main gas path thereby forcing some of the air into the bypass legs. The core flow then passes through a heater bank, a series of screens used for flow straightening, and finally into a two-dimensional converging section. In the vane cascade, two full passages were modeled with three vanes. A bleed is positioned on either side of the two-passage cascade to remove edge effects from the side walls while tailboards insure periodicity of the flow in the two passages.

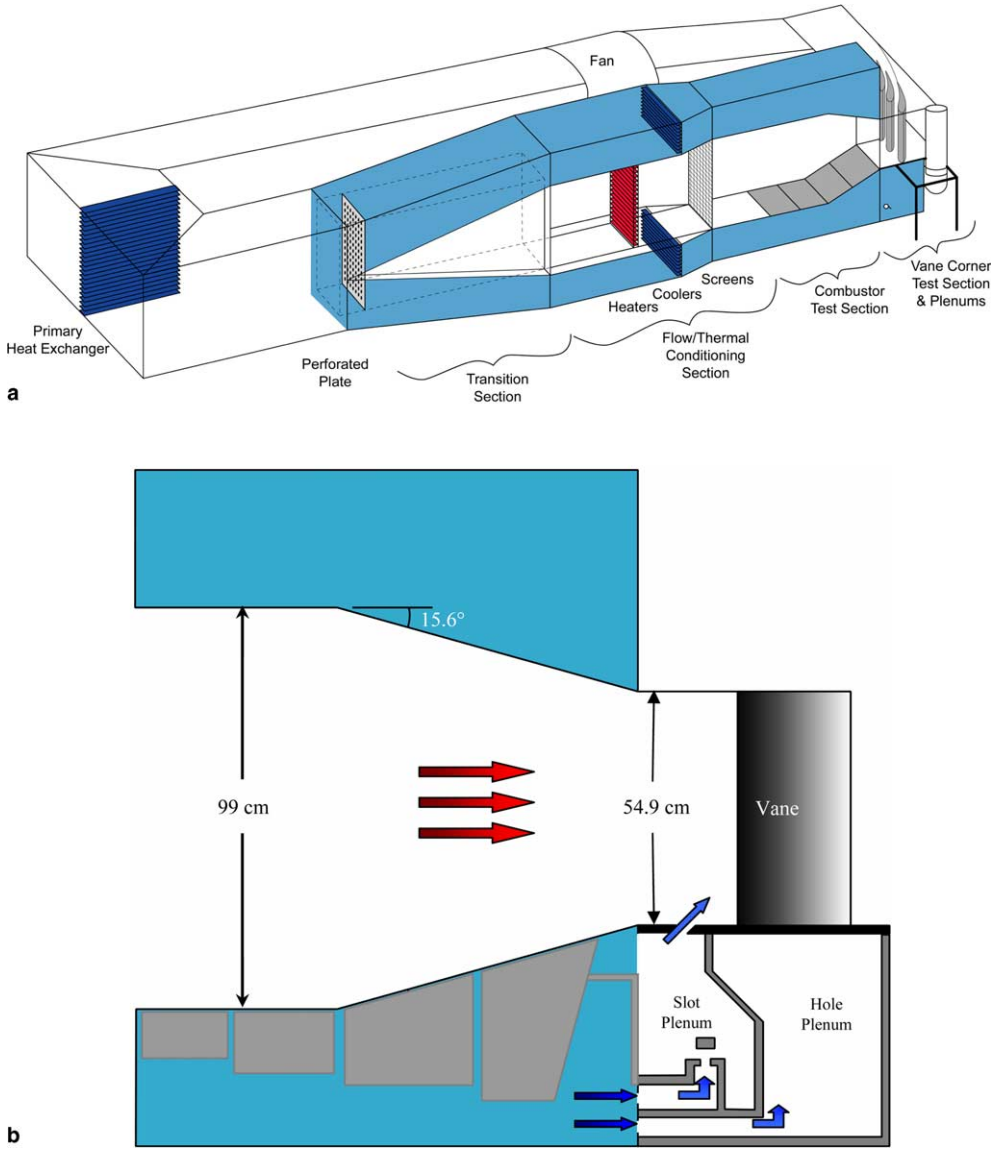

Fig. 5. (a) Illustration of wind tunnel facility. The flow is split into the primary channel and secondary channels before passing through the combustor simulator section and the vane cascade. (b) Cooling air from the bypass channel passes into the supply plenums through holes at the end of the combustor bypass. The cooling air is then injected into the passage through the slot or the holes where it interacts with the hot mainstream gases.

As was stated, this facility included three channels: a heated primary channel, representing the main gas path; and two symmetric secondary channels, representing the coolant flow paths. A 35–40 °C temperature differential between the coolant and mainstream was achieved by using the heaters in the primary channel and heat exchangers in the secondary channels. While the top secondary flow channel was closed off for these experiments, the bottom secondary flow channel was used for supplying the coolant to the slot and hole plenums, as seen in Fig. 5b. These two plenums were constructed to provide independent control of the slot and film-cooling flow rates. The front plenum supplied the slot flow while the rear plenum supplied the film-cooling flow. Typical times to achieve steady-state conditions were 3 h. As these experiments were to be relevant to industrial gas turbines where freestream turbulence levels can be lower than for aero-derivative engines, freestream turbulence effects were not the focus. The inlet turbulence level and length scales were measured, however,

to be 1.3% and 4 cm, respectively. The boundary layer approaching the slot was turbulent and measured to be 9% of the vane span. Note that the contraction just upstream of the vane is representative of that found in an actual gas turbine combustor section.

2.1. Cooling hole pattern and coolant flow settings

The vane geometry itself is described in Table 1. The cooling hole pattern that was considered for this study was one that was derived by industry and is representative of that for a first vane. This pattern is given in Fig. 6, which also indicates the location of the upstream slot between the combustor and turbine. In this study, coolant flow is also injected into the mainstream from this upstream flush slot. Specifics of the endwall and vane geometry are given in Table 2. All of the cooling holes have a 30° inclination angle while the arrows shown indicate the direction of the cooling jet injection. Fig. 6 also shows a gutter (marked with a G) that is located near the mid-passage of the endwall. This gutter was not considered for the current study but is there merely to indicate some of the rationale for locating the cooling holes. The gutter represents the mating location for adjacent vanes, which are generally cast in doublets or singlets with their associated platform.

Table 1
Summary of turbine vane geometry

Scaling factor	9
Scaled-up true chord length	59.4 cm
Pitch/true chord	0.77
Span/true chord	0.93
Re_{in}	2.3×10^5
U_∞	5.85 m/s
T_∞	20 °C
Inlet flow angle	0°
Trailing edge metal angle	72°

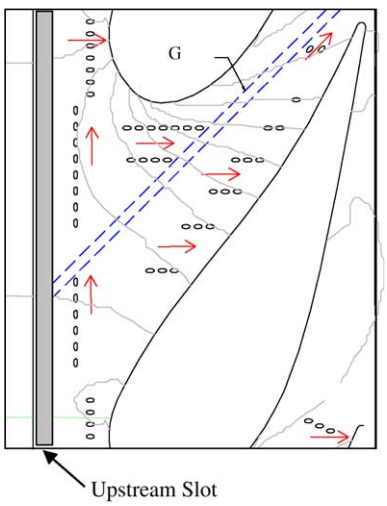

Fig. 6. Illustration of the upstream slot and film-cooling hole pattern. Note that the blue lines indicate the provision for a future study, but for this study was not included.

Table 2
Summary of endwall cooling hole and slot geometry

Feature	9X Scale
Cooling hole diameter (cm)	0.46
Cooling hole L/D	8.3
Hole injection angle	30°
P/D for leading edge holes	4/3
P/D for passage holes	3
Slot width (cm)	1.48
Slot length to width	1.8
Upstream slot location of vane	$-0.35C_a$
Slot injection angle	45°

For every test condition, the dimensionless pressure coefficient distribution was verified to insure periodic flows were set through the passages. Film coolant flow rates for each cooling hole could not be controlled since one plenum provided coolant to the entire endwall cooling hole pattern and the local static pressure field varied greatly from hole to hole. Friedrichs et al. [25] suggested that a global blowing ratio based on the inlet flow conditions could be characterized by the blowing ratio of a loss-free hole injecting into inlet conditions as calculated from:

$$M_{\text{ideal}} = \sqrt{\frac{\rho_c}{\rho_{in}} \cdot \frac{P_{0,c} - p_{s,in}}{P_{0,in} - p_{s,in}}} \tag{1}$$

A modification of this approach was taken for this study in that a global discharge coefficient, C_D, was derived so that the cumulative flow rate through the cooling holes could be characterized. The C_D values were obtained from CFD studies and have been previously reported by Knost and Thole [27]. Measurements of the inlet velocity, average inlet static pressure, and coolant total pressures were obtained which then allowed the fraction of coolant flow relative to the inlet core flow to be calculated from:

$$\frac{\dot{m}_c}{\dot{m}_{\text{core}}} = M_{\text{ideal}} \cdot C_D \cdot \frac{A_{\text{hole}}}{A_{in}} \cdot \#\text{holes} \tag{2}$$

A discharge coefficient of $C_D = 0.6$ was used for the slot flow. Note that for all of the experiments, the density ratio (jet-to-mainstream) was held fixed at 1.12.

2.2. Instrumentation and measurement uncertainty

The endwall test plate had a foam thickness of 1.9 cm (0.75 in), which was chosen because of its low thermal conductivity (0.033 W/m K) thereby providing nearly an adiabatic surface. To insure the precision and integ-

rity of the cooling hole pattern, the holes were cut with a five-axis water jet. An Inframetrics P20 infrared camera acquired the spatially-resolved adiabatic temperatures on the endwall. Measurements were taken at thirteen different viewing locations to insure that the entire endwall surface was mapped. From a camera distance of 55 cm, each picture covered an area that was 24 cm by 18 cm with the area being divided into 320 by 240 pixel locations. The spatial integration for the camera was 0.715 mm (0.16 hole diameters). The camera images were post calibrated using directly measured temperatures on the endwall by thermocouples that were installed. Thermocouple data was continuously acquired during image collection. The thermocouple measurements had a maximum to minimum range of approximately 0.8 °C with a standard deviation of 0.17 °C during the image collection time, which required about 30 min. For the post calibration the emissivity and background temperature were adjusted until the temperatures from the infrared camera images were within 1 °C of the corresponding thermocouple data. Typical emissivity values and typical background temperatures were 0.89 and 45 °C. Once the images were calibrated, the data was exported to an in-house Matlab program that was written for image assembly.

Three thermocouples were also located in both the slot and film-cooling plenums with one thermocouple beneath each of the passages and one beneath the center vane. These thermocouples allowed gradients in the coolant supply to be documented. Variation within the plenums was generally less than 0.3 °C. Voltage outputs from the thermocouples were acquired by a 32 channel data acquisition module that was used with a 12-bit digitizing card.

An uncertainty analysis was performed on the measurements of adiabatic effectiveness using the partial derivative method described at length by Moffat [32]. The precision uncertainty was determined by taking the standard deviation of six measurement sets of IR camera images with each set consisting of five images. The precision uncertainty of the measurements was ±0.014 °C. The bias uncertainty was ±1.0 °C based on the calibration of the image. The bias uncertainty of the thermocouples was ±0.5 °C. The total uncertainty was then calculated as ±1.0 °C for the images and ±0.51 °C for the thermocouples. The uncertainty in adiabatic effectiveness, η, was then found based on the partial derivative of η with respect to each temperature in the definition and the total uncertainty in the measurements. An uncertainty of $\partial\eta = \pm 0.0825$ at $\eta = 0.2$ and $\partial\eta = \pm 0.0292$ at $\eta = 0.9$ were calculated.

3. Results for slot injection of coolant

It is seen from Fig. 7a–c that increasing the amount of slot flow has a dramatic effect on the endwall adiabatic effectiveness levels (non-dimensional adiabatic surface temperatures). At the low 0.5% slot flow rate shown in Fig. 7a, the slot flow only exits in the middle of the passage with no coolant exiting just upstream of the vane leading edge. Note that these percentages refer to the coolant flow relative to the mainstream hot flow. As the slot flow is increased from 0.50% to 0.75%, shown

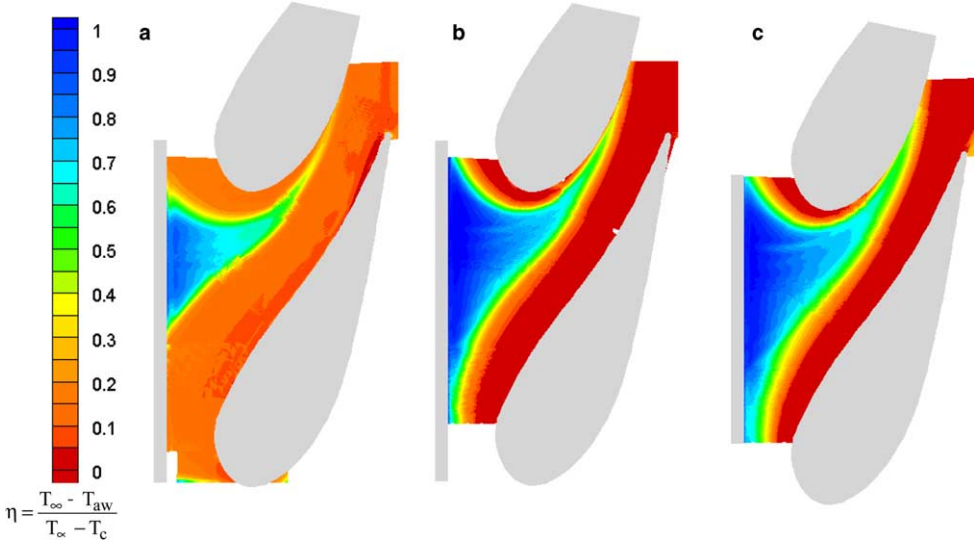

Fig. 7. Contours and pitchwise averages of adiabatic effectiveness for the cases of slot flow without film-cooling (a) 0.5%, (b) 0.75%, and (c) 1.0%.

in Fig. 7b, the coolant exits across the entire width of the slot still in a non-uniform manner. In both Fig. 7a and b, however, a large uncooled ring is left around the vane. This warm ring is especially evident in the stagnation region and along the pressure side. At the low slot flow the minimum effectiveness level is approximately 0.1 which corresponds to the measured near-wall dimensionless air temperature. This slight cooling effect of the near-wall fluid results from the long 4m, unheated boundary between the heater bank used to condition the core flow and the test section. At the increased blowing rate (Fig. 7b and c), the minimum effectiveness level is nearly zero. Increasing the slot flow results in the coolant exiting across the entire width of the slot and it then funnels towards the suction surface. The larger levels of near-wall coolant pulls the hotter mainstream gases onto the surface leading to a measured adiabatic effectiveness level of zero.

When the slot flow is doubled from the 0.5% to 1.0%, as shown in Fig. 7c, the coolant pattern is seen to be quite similar to the 0.75% case. The coolant, however, does slightly decrease the uncooled zone in the stagnation region, pushing the saddle point of the horseshoe vortex closer to the vane and narrowing the hot ring along the pressure side. The coolant at the highest flow rate also appears to impact the vane suction side slightly further upstream than in the 0.75% case. In all cases the slot flow exits in a non-uniform manner and is funneled between the legs of the horseshoe vortex towards the suction side.

Previous studies by Knost and Thole [28] indicated that the streamlines in the nearwall region, rather than the mid-span region, represent well the coolant flow paths. Predicted streamlines at the 2% vane span location for both the low and high slot flow cases are superimposed on the cooling hole pattern in Fig. 8 indicating the expected path traversed by jets emerging from the holes. It is seen that especially along the upstream portion of the pressure side and the upstream portion along the suction side to a lesser extent, the streamlines can be dramatically altered depending upon the slot flow rate. At a high slot flow rate, the streamlines are drawn towards the suction side of the vane more than at the low slot flow rate. This is apparent from the coolant contours in Fig. 7c, where for the high flow rate the coolant is convected closer to the vane.

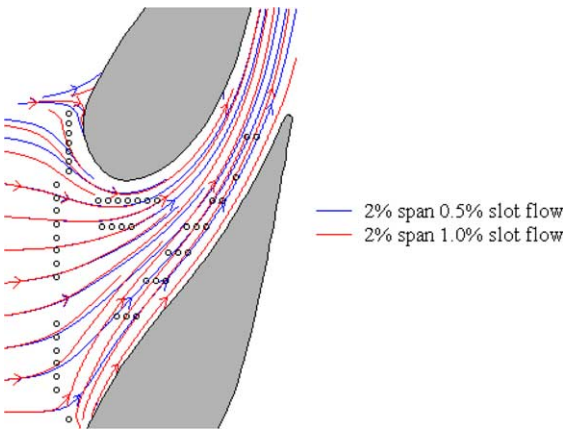

Fig. 8. Differences in near-wall streamlines for a range of slot flow condition.

4. Results for film-cooling studies

To assess the effect that the slot flow has on the film-cooling flow as well as the reverse, it was necessary to evaluate the adiabatic effectiveness levels for the film-cooling with no slot flow. The first row of cooling holes in the array of endwall film-cooling holes downstream of the slot will be referred to as the first row while the holes located immediately upstream of the vane will be referred to as the leading edge holes. This reference is illustrated in Fig. 9a.The two rows of holes located near the suction surface (near the top of the picture downstream of the leading edge holes) will be referred to as the suction side holes while the remainder of the rows of holes (near the pressure surface) will be referred to as the pressure side holes.

For the low blowing rate, shown in Fig. 9a, the most noticeable problem area is the large hot streak through the center of the passage. As was discussed previously, the minimum effectiveness levels are $\eta = 0.1$ for all cases because of the slightly cooler approaching boundary layer. The first row of holes inject with the streamlines despite being directed towards the top of the passage, although the local effectiveness levels are relatively low indicating partial jet separation. The first row of holes that are closer to the pressure surface (bottom of passage) inject in a merged group rather than individual jets. These merged jets are swept into the center of the passage providing some cooling to the center of the passage. The leading edge row of holes near the suction surface for this blowing rate provides relatively good cooling to the stagnation region where effectiveness levels are nominal values of 0.5. The pressure side holes in the passage do not appear to cool the region close to the vane-endwall junction resulting in a heated zone between the cooling holes and the vane.

The results of increasing the film-cooling flow rate are shown in Fig. 9b. Increasing the coolant flow for the same diameter cooling hole results in increased jet momentum that can lead to a separation from the surface in particular regions in the endwall. Separation of the jet is an undesirable condition because of the reduced cooling benefit on the wall that can result. This reduction is evident in comparing the effectiveness levels

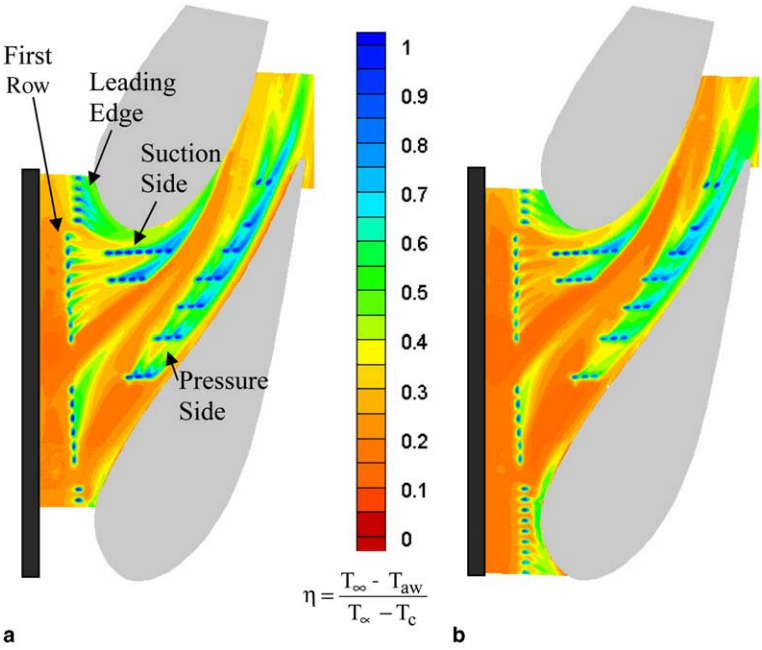

Fig. 9. Contours of adiabatic effectiveness for cases: (a) 0.5% film-coolant, (b) 0.75% film-coolant.

downstream of the first row of jets in Fig. 9a and b. The jet detachment in the first row of holes results in a stark reduction of cooling effectiveness.

Increasing the coolant for the leading edge row of holes produces an interesting result in Fig. 9b. Just downstream of the holes in the leading edge region, there are low levels of effectiveness which are then followed by high levels of effectiveness. This effectiveness pattern results from high momentum jets that separate from the wall, impinge upon the vane, and then are washed back onto the endwall surface. In comparing the momentum flux ratios for the jets in the leading edge regions for Fig. 9a and b, the low coolant flow case has a momentum flux ratio of 0.5 (Fig. 9a) to 2 (Fig. 9b). Except for the pressure side rows where there is an improvement of the cooling for the higher coolant flow conditions, Fig. 9a and b indicate a reduced cooling benefit for the higher coolant flow condition.

5. Results for combined slot flow and film-cooling

When placing film-cooling holes, a designer would like to predict the film-coolant trajectory to insure that the cooling needs of critical areas are met. A first approximation might be made by using a 2-D inviscid CFD prediction of the streamlines to predict the path of the coolant. This first approximation would not be correct as was indicated in Fig. 8 showing the large differences when comparing the flow turning angles for the two different slot flow conditions (2-D would imply mid-span values rather than near-wall values which can vary widely). Further examination of these turning angles indicate the cross flows that are induced in the near wall region for a high slot flow have deviations from the midspan by as much as 40° near the stagnation location.

Predicted streamlines in the near wall region (2% span) with slot flow but without film-cooling are shown superimposed on adiabatic effectiveness measurements in Fig. 10a–c for a range of slot flow conditions (0.5%, 0.75%, and 1%) at a given film-cooling flow (0.5%). Comparing these contours allows one to assess the effect that the slot flow has on the film-cooling flow.

As the slot flow is increased while the film-cooling flow is maintained at 0.5%, it is seen from Fig. 10a–c that the slot coolant coverage is dramatically increased as was the case with no film-cooling. At the 1% condition, coolant exits across the entire width of the slot, but is still funneled towards the suction side. Adiabatic effectiveness levels across much of the upstream portion of the endwall are nearly unity indicating overcooling by the slot. The leading row of holes over a large portion of the pitch appears to be unnecessary for endwall cooling. Therefore, the coolant emerging from these holes could be redistributed to more advantageous locations.

The film-coolant trajectories in Fig. 10a–c follow the predicted streamlines quite well in a number of loca-

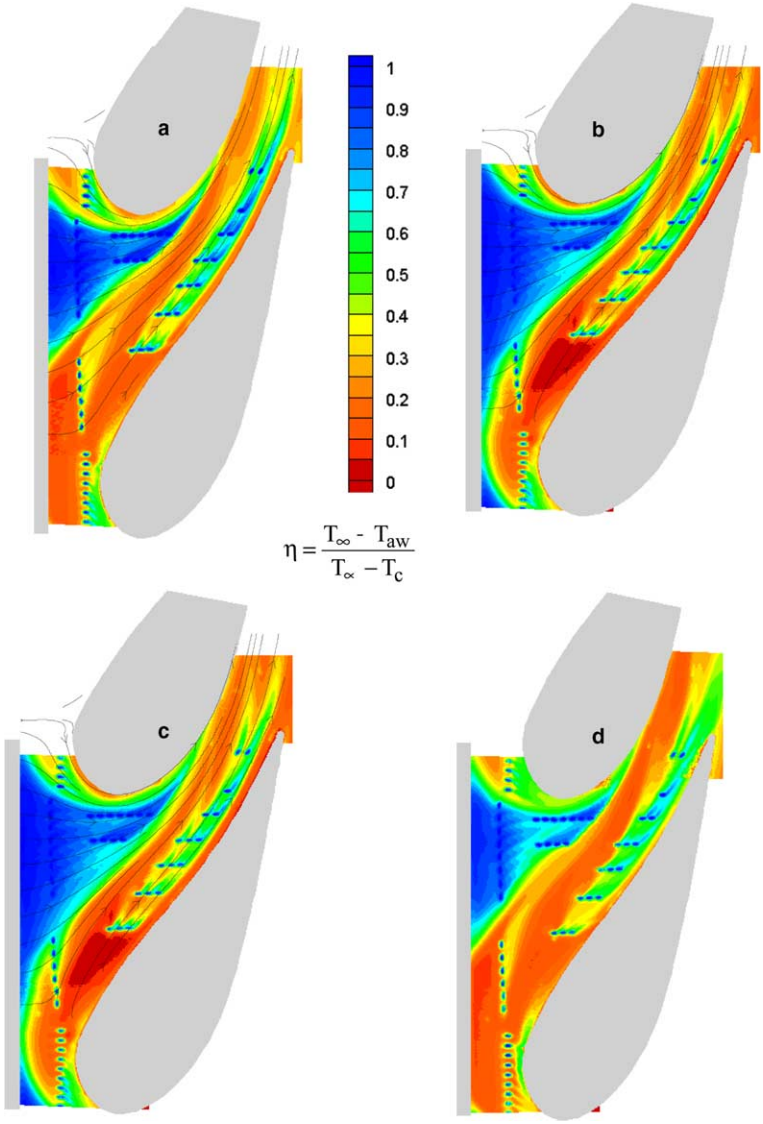

Fig. 10. Contours of adiabatic effectiveness for (a) 0.5% film-cooling and 0.5% slot, (b) 0.5% film-cooling and 0.75% slot flow, (c) 0.5% film-cooling and 1% slot flow, and (d) 0.75% film-cooling and 0.5% slot flow.

tions. The coolant from the holes in the stagnation region is swept around the suction side and the jets along the pressure side of the vane follow the predictions. The largest difference between the streamlines and the coolant trajectory is in the leading row of holes near to the pressure side of the vane, which is outside of the slot coolant flow but is clearly being affected by the slot flow. This location shows that the holes are directed in a strong cross-pitch direction than the predicted streamlines would indicate. The trend, however, is predicted correctly with the higher slot flows resulting in these jets being directed more towards the suction surface. The adiabatic effectiveness contours for the leading edge row of holes near the pressure side also show that these jets are being entrained increasingly as the slot flow increases.

To address whether the film-cooling flow has an effect on the slot flow, compare Fig. 10a (0.5% film-cooling and 0.5% slot flow) and 10d (0.75% film-cooling and 0.5% slot flow). The contours do not indicate strong effects of the increased film-cooling flow on the slot flow, but there is a widening of the uncooled region between

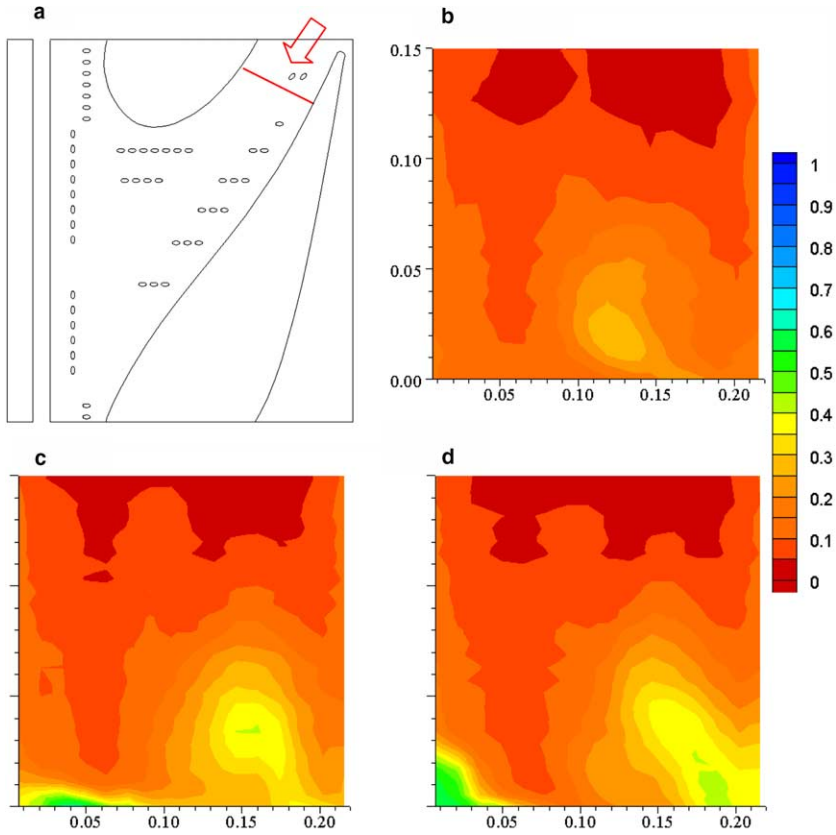

Fig. 11. Thermal field data was acquired in (a) a plane normal to the pressure surface at $s/C_a = -0.77$. Contours of non-dimensional temperature are shown for (b) 0.5% slot flow without film-cooling, (c) 0.5% slot flow with 0.5% film-cooling, and (d) 0.5% slot flow with 0.75% film-cooling.

the jets as the jets become more directed. To further examine this trend, comparisons were made of the measured thermal fields in a plane shown in Fig. 11a. This measurement plane is normal to the pressure side at $s/C = -0.77$ and extends across the passage to the adjacent vane. The plane is viewed from downstream as indicated by the arrow so that the pressure side is on the left at $y/P = 0$ and the suction side of the adjacent vane is on the right.

For the 0.5% slot flow case without film-cooling, shown in Fig. 11b, the coolant is entrained in the passage vortex and transported across the passage to the suction side. The core of the coolant is located above the endwall at 2% span with some coolant extending down to the endwall. The combined low slot and film case is shown in Fig. 11c. Once again the core slot flow is entrained in the passage vortex and transported across the passage. A slightly cooler center is seen most likely resulting from the additional coolant added by the cooling jets. The slot core is also lifted slightly and shifted further towards the suction side by the stronger secondary flows resulting from coolant injection. The pressure side jets are seen at approximately $y/P = 0.04$ (near the suction surface). These jets adhere relatively well to the endwall surface. Finally, the increased blowing rate with the 0.5% slot flow is shown in Fig. 11d. The slot flow, as seen before, is entrained in the passage vortex and transported towards the suction side. The passage vortex, indicated by the thermal field contours, result in a skewed shape, as a result of the increased blowing with less convection of the passage vortex towards the suction surface. The pressure side jets indicate that the coolant is climbing onto the vane surface with the higher film-cooling flow. It is also evident from comparing the thermal field contours in Fig. 11b and d that the hot streak along the endwall has widened given the more directed jets.

6. Conclusions

Measurements of adiabatic effectiveness were presented for an extensive test matrix combining both coolant from a flush slot and film-cooling distinct cooling

holes in the endwall of a turbine vane. The most important conclusion that can be drawn from this work is the influence that upstream condition has on the secondary flows that develop in a turbine passage. This is particularly important when considering slot leakage flows, which are inherently present when mating the turbine and the combustor.

With upstream slot cooling alone, there were many regions that remained uncooled along the endwall as was indicated by a ring around the entire vane with no coolant present. The coolant flow was found to exit the slot in a non-uniform manner with most of the flow exiting at the mid-passage between the vanes. Predicted streamlines at 2% span that included slot flow were compared and it was found that as the slot flow rate was increased the near-wall streamlines indicate a stronger turning toward the suction surface. These results show it is even more critical as to the inclusion of the slot flow at the high coolant flowrates.

With the combined film-cooling and slot flow cases, it was noted that a large portion of the mid-passage region along the endwall required no additional cooling holes since it was sufficiently cooled in many of the cases with the slot flow alone. Effects that the slot flow had on the film-cooling were shown to primarily be the effect described previously with stronger crossflows at the higher slot flows. For the same slot flow with increased film-cooling flow, thermal field measurements indicated that there was a change in the passage vortex. As the film-cooling flowrates were increased, the jets became more directed widening the uncooled portion of the endwall.

References

[1] C.H. Sieverding, Recent progress in the understanding of basic aspects of secondary flows in turbine blade passages, J. Eng. Gas Turbines Power 107 (1985) 248.

[2] W.R. Hawthorne, Secondary circulation in fluid flow, Proc. Roy. Soc. A 206 (1951) 374.

[3] L.S. Langston, Crossflows in a turbine cascade passage, J. Eng. Power 102 (1980) 866.

[4] O.P. Sharma, T.L. Butler, Predictions of endwall losses and secondary flows in axial flow turbine cascades, J. Turbomachinery 109 (1987) 229.

[5] R.J. Goldstein, R.A. Spores, Turbulent transport on the endwall in the region between adjacent turbine blades, ASME J. Heat Transfer 110 (1988) 862–869.

[6] D.A. Bailey, Study of mean- and turbulent-velocity fields in a large-scale turbine-vane passage, ASME J. Eng. Power 102 (1980) 88–95.

[7] J. Moore, D.M. Schaffer, J.G. Moore, Reynolds stresses and dissipation mechanisms downstream of a turbine cascade, ASME J. Turbomachinery 109 (1987) 258–267.

[8] D.G. Gregory-Smith, J.G.E. Cleak, Secondary flow measurements in a turbine cascade with high inlet turbulence, J. Turbomachinery 110 (1992) 1–8.

[9] M. Kang, K.A. Thole, Flowfield measurements in the endwall region of a stator vane, J. Turbomachinery 122 (2000) 458–466.

[10] M. Suo, Turbine cooling, in: G.C. Oates (Ed.), Aerothermodynamics of Aircraft Engine Components, AIAA, Inc. publisher, 1985.

[11] B.A. Halls, Nozzle Guide Vane Cooling, AGARD, CP No. 73, Paper 25, 1970.

[12] S.C. Crocker, D. Nickolaus, C.E. Smith, CFD Modeling of a Gas Turbine Combustor from Compressor Exit to Turbine Inlet, ASME Paper 98-GT-184.

[13] B. Lakshminarayana, Effects of inlet temperature gradients on turbomachinery performance, ASME J. Eng. Power 97 (1975) 64.

[14] K. Hermanson, K.A. Thole, Effect on non-uniform inlet conditions on endwall secondary flows, J. Turbomachinery 124 (2002) 623–631.

[15] W.F. Colban, A.T. Lethander, K.A. Thole, G. Zess, Combustor-turbine interface studies: Part 2: Flow and thermal field measurements, J. Turbomachinery 125 (2002) 203–209.

[16] M. Kang, A. Kohli, K.A. Thole, Heat transfer and flowfield measurements in the leading edge region of a stator vane endwall, J. Turbomachinery 121 (3) (1999) 558–568.

[17] M.F. Blair, An experimental study of heat transfer and film cooling on large-scale turbine endwalls, J. Heat Transfer (November) (1974) 524–529.

[18] D. Granser, T. Schulenberg, Prediction and measurement of film cooling effectiveness for a first-stage turbine vane shroud, ASME Paper Number 90-GT-95, 1990.

[19] L. Zhang, H.K. Moon, Turbine nozzle endwall inlet film cooling—The effect of a back-facing step, GT-20030-38319.

[20] H. Pasinato, K. Squires, R.P. Roy, Measurements and modeling of the flow and heat transfer in a contoured vane-endwall passage, Int. J. Heat Mass Transfer 47 (2004) 5685–5702.

[21] S.W. Burd, T.W. Simon, Effects of slot bleed injection over a contoured endwall on nozzle guide vane cooling performance: Part I: Flow field measurements, ASME Paper No. 2000-GT-199.

[22] S.W. Burd, C.J. Satterness, T.W. Simon, Effects of slot bleed ijection over a contoured endwall on nozzle guide vane cooling performance: Part II: Thermal measurements, ASME Paper No. 2000-GT-200.

[23] R. Oke, T. Simon, S.W. Burd, R. Vahlberg, Measurements in a turbine cascade over a contoured endwall: discrete hole injection of bleed flow, ASME Paper Number 2000-GT-214.

[24] S. Friedrichs, H.P. Hodson, W.N. Dawes, Distribution of film-cooling effectiveness on a turbine endwall measured using the ammonia and diazo technique, J. Turbomachinery 118 (1996) 613–621.

[25] S. Friedrichs, H.P. Hodson, W.N. Dawes, Aerodynamic aspects of endwall film-cooling, J. Turbomachinery 119 (1997) 786–793.

[26] S. Friedrichs, H.P. Hodson, W.N. Dawes, The design of an improved endwall film-cooling configuration, J. Turbomachinery 121 (1999) 772–780.

[27] D.K. Knost, K.A. Thole, Computational predictions of endwall film-cooling for a first stage vane, GT-2003-38252.

[28] D.G. Knost, K.A. Thole, Adiabatic effectiveness measurements of endwall film-cooling for a first stage vane, J. Turbomachinery 127 (2005).
[29] F. Kost, M. Nicklas, Film-cooled turbine endwall in a transonic flow field: Part I – Aerodynamic measurements, J. Turbomachinery 123 (2001) 720–729.
[30] M. Nicklas, Film-cooled turbine endwall in a transonic flow field: Part II—Heat transfer and film-cooling effectiveness measurements, J. Turbomachinery 123 (2001) 720–729.
[31] M.D. Barringer, O.T. Richard, J.P. Walter, S.M. Stitzel, K.A. Thole, Flow field simulations of a gas turbine combustor, J. Turbomachinery 124 (2002) 508–516.
[32] R.J. Moffat, Describing the uncertainties in experimental results, Exp. Thermal Fluid Sci. 1 (1988) 3–17.